Magnetic structure and critical properties of $FeGe_2$

L. M. Corliss, J. M. Hastings, W. Kunnmann, R. Thomas, and J. Zhuang*
Department of Chemistry, Brookhaven National Laboratory, Upton, New York 11973

R. Butera
Department of Chemistry, University of Pittsburgh, Pittsburgh, Pennsylvania 16701

D. Mukamel
Department of Physics, The Weizmann Institute of Science, Rehovot, Israel
(Received 24 September 1984)

A neutron study of the tetragonal antiferromagnet $FeGe_2$ has shown the existence of two continuous magnetic transitions at temperatures of ~ 263 and ~ 289 K. The upper temperature corresponds to a transition from paramagnetism to a basal-plane spiral structure propagating along the cell edges in that plane. At the lower temperature the spiral structure is transformed into the simple collinear structure previously reported in the literature. Typical critical behavior is observed at the upper temperature for individual satellite peaks. The spiral propagation vector decreases continuously to zero at the lower critical point, exhibiting power-law behavior with an exponent of $0.40_7 \pm 0.005$. Heat-capacity measurements reveal two λ-type anomalies with critical exponents in the expected range. The phase diagram has been analyzed using mean-field and renormalization-group considerations. A model based on zero basal-plane spin anisotropy yields a magnetic structure which agrees with the observed structure of the intermediate phase. The effect of an external field has also been treated theoretically.

I. INTRODUCTION

The magnetic properties of $FeGe_2$ have been extensively studied but have not been satisfactorily related to magnetic structure. The present study reports new information on the magnetic structure, its temperature dependence, and critical point properties, which can provide a basis for interpreting physical measurements.

$FeGe_2$ crystallizes with the tetragonal ($C16$) structure[1] ($a = 5.908$ Å, $c = 4.955$ Å) shown in Fig. 1, in which layers of Fe atoms alternate with layers of Ge atoms. Its magnetic properties were first studied by Yasukochi *et al.*,[2] who reported it to be antiferromagnetic and weakly ferromagnetic below 190 K. The antiferromagnetism was confirmed in the work of Airoldi and Pauthenet,[3] but in this, as well as in later work, no evidence of ferromagnetism was found.

A powder neutron diffraction study by Krén and Szabó[4] gave the magnetic structure indicated in Fig. 1, but the accuracy was not sufficient to give both the moment and the orientation of the antiferromagnetic axis. A basal plane configuration was suggested inasmuch as this gave a value for the iron moment of $1.2\mu_B$, which is close to that found in the isostructural compound $FeSn_2$.

A powder neutron diffraction study by Krén and Szabó[4] gave the magnetic structure indicated in Fig. 1, but the accuracy was not sufficient to give both the moment these authors concluded that the structure was noncollinear with a configuration that can be visualized using Fig. 1, by rotating the spin axis at $z = \frac{1}{2}$ through an angle of $71° \pm 6°$ about c with respect to that at $z = 0$. The powder intensities were regarded as too weak to give reliable structure information. The temperature dependence of the peak intensity of the (100) antiferromagnetic reflection showed the rapid decline expected for a second-order magnetic transition together with a tail attributed to

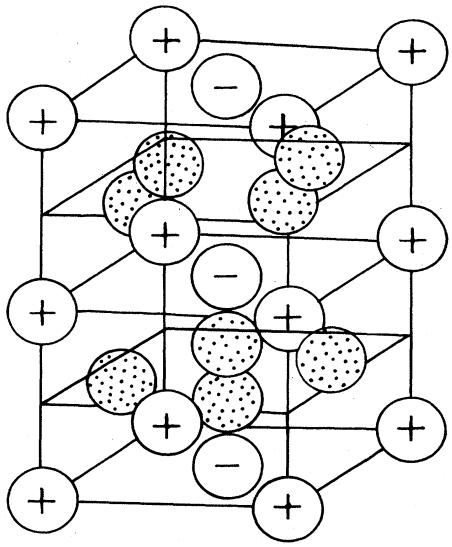

FIG. 1. Crystal structure of $FeGe_2$. Ge atoms are represented by dotted circles and Fe by open circles. Plus and minus signs refer to the collinear spin structure first suggested by Krén and Szabó (Ref. 4).

short-range order. The steep part of the curve extrapolated to ~270 K, whereas the tail extended to between 285 and 290 K. Mössbauer measurements performed by these authors gave a Néel point of 287±2 K, based on the disappearance of the hyperfine field. The discrepancy between this value and that given by magnetic scattering measurements was thought to be associated with the high degree of short-range order above ~270 K.

Independent powder neutron studies by Satya Murthy *et al.*,[6] Bertaut and Chenavas,[7] and Adelson and Austin,[8] confirmed the collinear model with the spin in the basal plane and the magnitude of the moment equal to $(1.2\pm0.1)\mu_B$. Bertaut and Chenavas[7] pointed out that of the reflections predicted by the noncollinear model of Forsyth *et al.*[5] should have been visible in the powder diagrams, but was not observed. They concluded that the single crystals might have been been chemically different from the powder and suggested further study.

Sólyom and Krén[9] reviewed the various proposals for the magnetic structure, pointing out that according to the Landau theory of second-order transitions, only collinear structures were allowed, with moments directed along the tetragonal axis or along either [100] or [110] in the basal plane. They suggested three possibilities. (1) The transition is not second order. (2) The noncollinear structure is associated with two successive second-order transitions, with the first giving rise to a collinear structure and the second to a structure, such as that proposed by Forsyth *et al.*,[5] having two components, each of which has an allowed symmetry. (3) The interpretation of the single-crystal measurements is erroneous.

This analysis was followed by a series of papers reporting anomalies in a variety of physical properties which could be associated with two successive transitions. Krentsis *et al.*[10] measured the temperature dependence of resistivity, thermoelectric power, and linear expansion coefficients, using crystals cut in the [001] and [100] directions, and observed distinct anomalies at two temperatures. Mikhel'son *et al.*,[11] using the same samples, measured the variation with temperature of the specific heat and also the susceptibility along [001] and [110]. The specific heat exhibited two fairly sharp maxima at 265 and 285 K in agreement with magnetic transitions observed in $\chi_{[110]}$. Mössbauer measurements were carried out by Sachkov *et al.*[12] on single crystals at 242 K. They reported that line intensities agreed best with the model of Forsyth *et al.*,[5] but as in the work of these authors, the spectra showed no evidence of a transition at 265 K. The anisotropy observed in the basal-plane spectra was explained on the basis that the thin crystal plates were single domain. Proceeding from this idea, the authors suggested that the apparent transition observed at ~265 K for bulk single crystals and powders represented a domain reorientation. The results obtained in this Mössbauer study induced Piratinskaya *et al.*[13] to carry out a more detailed investigation of the anisotropy of the magnetic susceptibility. The behavior of the low-temperature susceptibility along various symmetry directions was explained in terms of the noncollinear model, using the idea of domains and making assumptions about the easy magnetic axes. No explanation was offered, however, for the abrupt changes in $\chi_{[100]}$ and $\chi_{[110]}$ near 260 K and for the disappearance of basal-plane anisotropy above that temperature.

Zinov'eva *et al.*[14] studied the temperature dependence of the velocities of longitudinal and transverse ultrasonic waves in single-crystal specimens, and reported anomalies at two temperatures. The discontinuities in compressibility obtained from elastic constants near 287 K, taken together with previously determined discontinuities in specific heat and thermal expansion were found to satisfy Belov's relation[15] for a second-order transition. In confirmation of this characterization of the transition, the change in the velocity of sound waves was found to exhibit a power-law dependence on temperature in the vicinity of 287 K, as predicted by Bennett.[16] More recently, ultrasonic attenuation anomalies were studied by Pluzhnikov *et al.*,[17] using crystals also grown at the Kirov Polytechnic Institute, Sverdlovsk. The lower transition was found to exhibit thermal and stress hysteresis and was judged to be first order. It was not found possible, however to characterize satisfactorily the transition at T_N.

II. SAMPLE PREPARATION

Two large ingots (50 g, 110 g) of $FeGe_2$ were prepared by fusion, in evacuated silica tubes, of a stoichiometric mixture of "spectroscopically pure" iron rod and 99.9995 + % grade germanium, at 975 °C for several days, using an MgO crucible to contain the melt. Since the compound is quite brittle, the ingots were readily crushed and remelted to ensure maximum reaction. After the remelting procedure, the smaller ingot was crushed (not ground) to a fine powder and sealed *in vacuo* in a silica tube, which, in turn, was inserted into a length of heavy-walled copper pipe, to minimize temperature gradients. The ends of the pipe were plugged with "quartz wool" and the assembly sealed under vacuum in a large silica tube. This assembly was heated to 550 °C for several days and then slow-cooled (80 °C/day) to room temperature. This annealed, finally divided sample was used for neutron powder measurements. The larger ingot, prepared for use in the heat-capacity measurements, was similarly treated, but crushed only to a particle size range of 1—5 mm prior to annealing.

Utilizing a portion of the fine powder, a modified Bridgman technique was used to grow large ($\frac{1}{4}\times3$ in.) rods of $FeGe_2$ (mp ~866 °C) in a shaped, recrystallized alumina crucible, contained in an evacuated silica tube. The conventional technique was modified to maintain the bottom tip of the crucible approximately 200 °C cooler than the rest of the melt in order to prevent supercooling into a metastable eutectic. Single-crystal specimens were cleaved from the rods.

Slow vapor-phase growth of $FeGe_2$ crystals was found to occur when a small amount of $FeGe_2$ powder was sealed under I_2 vapor in an otherwise evacuated silica tube and placed in a horizontal tube furnace in a way that produced a temperature gradient of approximately 50 °C along the length of the tube. It was observed that transport of $FeGe_2$ solid occurred in the direction of cold to hot in the temperature range 500 °C to 725 °C, as measured at the hot end of the tube. At higher temperatures a re-

versal of transport direction occurred even for gradients of 20°C or less. Crystals grown at, or very close to, the inversion point are expected to be stoichiometrically equivalent to the original powder charge, and indeed, crystals grown under these conditions showed excellent facial development.

III. LOW-TEMPERATURE STRUCTURE

The noncollinear structure of Forsyth *et al.*[5] was deduced from the appearance at low temperatures of two sets of extra reflections: type 1, with $h+k$ odd and l odd, and type 3, with $h+k$ odd and l even. The type-3 reflections are those observed in all the powder neutron studies, whereas type-1 reflections were observed only with single crystals. The initial experience in the present work was the same as that of earlier workers and a number of experiments were performed to clarify the difference between single crystals and powders. In the first of these experiments, the temperature dependence of the (100) reflection (type 3) was compared with that of the (101) and (103) reflections (type 1), using a single crystal of approximately 10 mm^3 in volume. Whereas the (100) decreased in typical Brillouin fashion, the (101) and (103) were essentially constant in the same temperature interval, suggesting, at the very least, that they were not associated with the same magnetic structure. In a second experiment, a very small perfect crystal with typical linear dimensions of 0.1 mm was grown by vapor transport and oriented with x rays to facilitate the location of reflections with neutrons. This crystal exhibited a (100) reflection (type 3), but *not* the (101) which is of type 1. A large single crystal with a volume of ~ 5 cm^3 and which exhibited prominent type-1 reflections, was then ground into a powder and reexamined. The powder pattern showed only type-3 reflections. These experiments strongly suggested that type-1 reflections were spurious and were produced by double-Bragg nuclear scattering, which is allowed for type 1, but not for type 3. This suspicion was confirmed by studying the variation of the (101) intensity as a function of incident wavelength and observing that it was reduced essentially to zero by a 10% change in wavelength. [Nuclear double-Bragg scattering would produce an apparent peak at the (101) position if the (101) and a suitable second reciprocal-lattice point were simultaneously located on the Ewald sphere of reflection. This geometrical coincidence, if accidentally realized, can be destroyed by varying the wavelength and hence the radius of the sphere.]

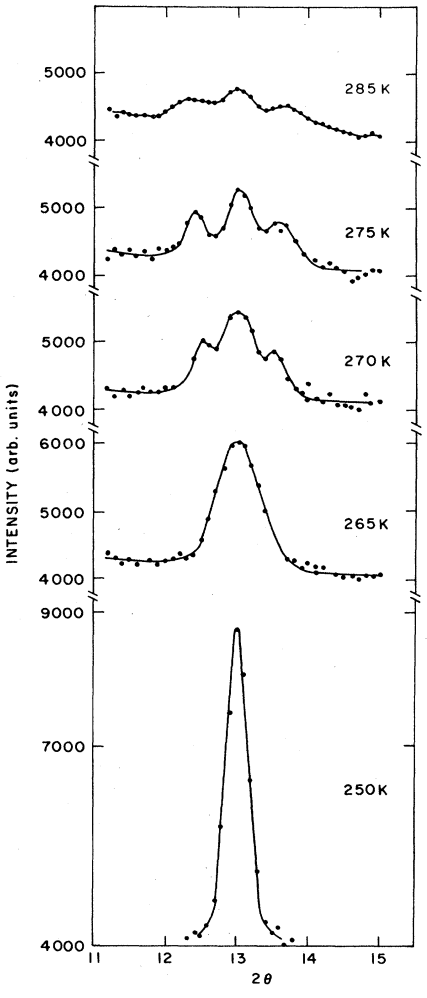

FIG. 2. Powder diffraction scans of the (100) magnetic reflection showing the sharp line, characteristic of the low-temperature structure, and the splitting associated with the intermediate phase.

We thus conclude that the low-temperature structure of $FeGe_2$ is, in fact, the collinear one suggested by the several powder studies and shown in Fig. 1. It is difficult, however, to obtain both the magnitude and orientation of the spins from powder data. The single-crystal data of Forsyth *et al.*[5] for the type-3 reflections show most clearly that the spins have magnitude $1.2\mu_B$ and are confined to the basal plane.[18]

IV. INTERMEDIATE PHASE

The magnitude behavior at higher temperatures can be seen qualitatively in the powder diffraction scans of the (100) magnetic reflection shown in Fig. 2. At 250 K the peak is sharp, with an angular width of 0.4° determined by the instrumental resolution. At 265 K the peak is broadened to 0.75° and at 270 K a definite splitting is observed. This splitting increases with increasing temperature and at 285 K, in the vicinity of the Néel point, individual components are noticeably broadened. The splitting is clearly seen in single crystal scans of the magnetic reflections, as illustrated in Fig. 3. (To perform this type of scan, the scattering vector is advanced in uniform steps through the reciprocal-lattice point in a direction parallel to a^*.)

A detailed mapping of reciprocal space in the temperature regime where splitting occurs showed the presence of four spots of equal intensity, located symmetrically in [100] and [010] directions about reciprocal-lattice points corresponding to the low-temperature structure. At these temperatures the low-temperature phase is evidently modulated with equivalent propagation vectors along the [100] and [010] directions. The determination of the dis-

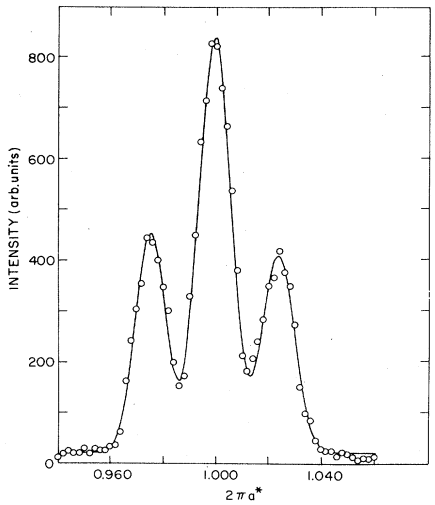

FIG. 3. Single-crystal scan of the (102) magnetic reflection at 265 K. The a^*c^* reciprocal plane is horizontal and scan direction is parallel to a^*. The line is a least-squares fit to the data using a Gaussian line shape.

tribution of satellite spots is illustrated in Fig. 4 for the case of a scan through the (100) reciprocal-lattice point in the [100] direction, with the a^*c^* plane horizontal. [In this configuration, two spots are in the scattering plane along a^* on either side of (100) and two are located in the b^* direction above and below the scattering plane.] The scan in Fig. 4(a) was made with tight vertical resolution so that the vertically displaced spots were not detected and consequently the central component seen in Fig. 3, for example, was absent. The crystal was then tipped to bring one of the vertical spots into the plane of diffraction while simultaneously displacing the two spots that were previously in diffracting position. In Fig. 4(b) one sees the presence of a central spot contributed by one of the two out-of-plane satellites and the virtual disappearance of the two spots seen before. The intensities of the individual peaks in Figs. 4(a) and 4(b) are essentially equal. The equality of the satellite spots is also seen in Fig. 3 where, with ordinary vertical resolution, the two vertically displaced spots are superimposed to form the central peak of the scan, with a combined intensity equal to twice that of each of the side peaks.

A pattern of four equal satellites requires spin modulation propagated along both the [100] and [010] directions. This can be achieved with flat basal plane spirals or with independent transverse and longitudinal spin-density waves propagating along each of these directions. These possibilities will be discussed in detail in Sec. VIII. A third possibility, in which spins are oriented along the c axis, with magnitudes modulated in the [100] and [010] directions, is rejected because it fails to account for the observed ratio of the intensities of the (102) and (100).

V. LOW-TEMPERATURE TRANSITION

The magnitude of the propagation vector of the modulated structure, $2\pi\mathbf{k}$, is given by one-half the separation of a pair of symmetrically disposed satellite peaks in units of

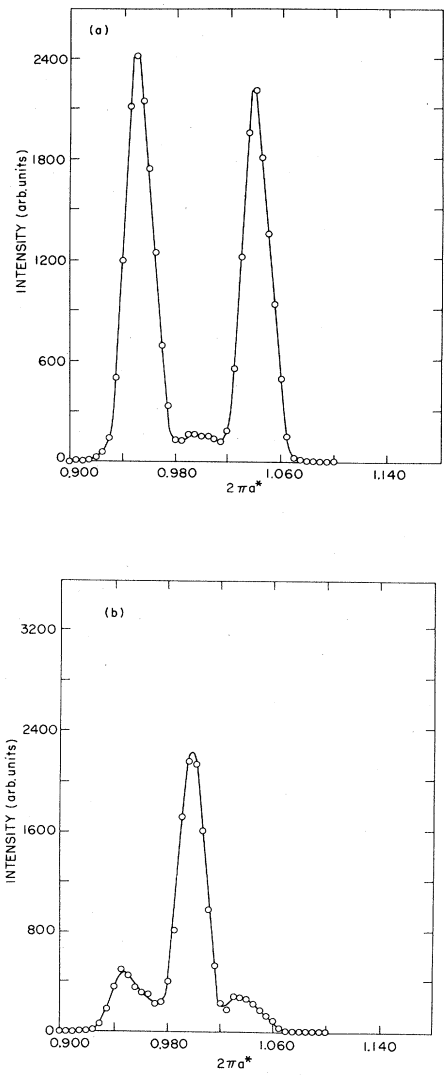

FIG. 4. (a) Scan of (100) magnetic reflection at 275 K with tight vertical collimation. The a^*b^* plane is horizontal and the scan direction is along a^*. (b) Repeat of scan in (a) with crystal tipped to permit observations of a single vertically displaced satellite.

$2\pi a^*$, the reciprocal-axis length. This separation was measured as a function of temperature in the region of the (102) reciprocal-lattice point, with the a^*c^* plane horizontal and the direction of scan parallel to a^*. Over the temperature range from 285 to 262.7 K, this separation decreased continuously, requiring progressive improvement in the instrumental resolution. Comparison of results obtained at the same temperature with different instrumental configurations were carried out to ensure that these changes in resolution did not influence the observed peak separation. Positions of individual satellite peaks were obtained from least-squares fits of the experimental scans using Gaussian line shapes. The quality of the fit obtained in this way can be seen in Fig. 3.

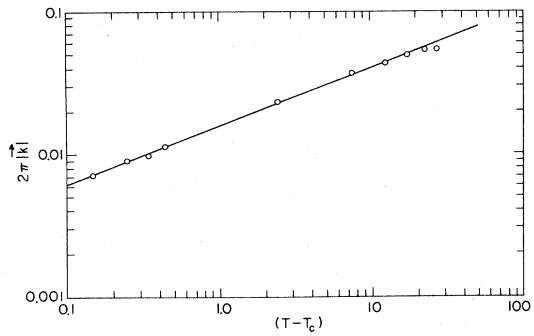

FIG. 5. Log-log plot of the temperature dependence of the magnitude of the propagation vector for the spiral spin structure. The exponent β_k, given by the slope, is $0.40_7 \pm 0.005$; T_c, the low-temperature transition point is 265.55 K.

The magnitude of the propagation vector was found to follow quite closely a power-law dependence on temperature:

$$2\pi |\mathbf{k}| = c_k (T - T_c)^{\beta_k}$$

with a transition temperature $T_c = 262.55$ and $\beta_k = 0.40_7 \pm 0.005$. A log-log plot of this equation is given in Fig. 5. It is quite remarkable that linearity is observed over essentially the whole temperature range in which the modulated structure is stable. Attempts to detect possible thermal hysteresis in the temperature dependence of the propagation vector were inconclusive; an upper limit was estimated to be approximately 0.1 K (0.04%).

VI. NÉEL POINT TRANSITION

The planar configuration of four equal satellite spots is maintained up to the Néel point. The intensity associated with individual spots was found to decrease continuously as T_N was approached and critical scattering typical of second-order transitions was observed near T_N, centered

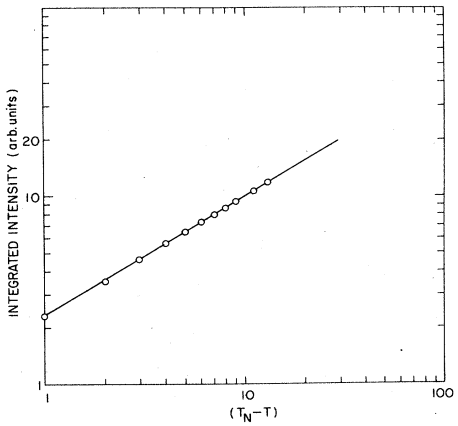

FIG. 6. Log-log plot of the integrated Bragg intensity of a single satellite reflection as a function of temperature near the Néel point. The line is drawn for $2\beta = 0.64 \pm 0.01$ and $T_N = 288$ K.

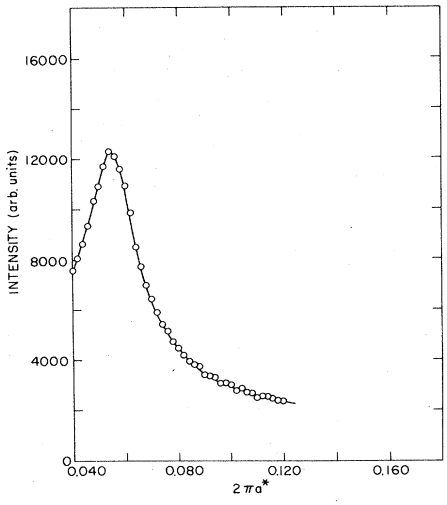

FIG. 7. Critical scattering associated with a single satellite reflection at 290.0 K.

at each satellite position. The temperature dependence of the integrated intensity of an individual satellite reflection was measured at the (010) position, with the c axis vertical, by scanning in the [100] direction. Just below T_N, the satellites are well separated and intensity measurements were straightforward. The results, corrected for critical scattering, are represented in the log-log plot of Fig. 6, using an experimental value of T_N given by the temperature at which the critical scattering was a maximum. The value of 0.64 ± 0.01 for 2β is seen to be typical of values observed for Heisenberg antiferromagnets in second-order phase transitions.

The critical scattering above T_N, and its temperature dependence, were more difficult to determine because of overlap of the Lorentzian tails associated with different satellites. Typical data for the region least affected by this overlap is shown in Fig. 7. Values of the inverse range parameter κ were obtained for several temperatures by least-squares fitting with a Lorentzian cross section convoluted with the instrumental resolution function. The data are of limited accuracy but nevertheless provide strong confirmation of second-order behavior. A log-log plot of κ versus $(T - T_N)^{\nu}$, shown in Fig. 8, yields a rough value for the exponent ν of 0.72 ± 0.08, which is in the expected range. The Néel point used to construct Fig. 8 was taken as the point where the data could no longer be satisfactorily represented by a Lorentzian owing to the superposition of Bragg scattering at the center of the scan. The independently determined values of T_N used to obtain β and ν, differ by approximately 0.5%. This is larger than one would like for a quantitative determination, but small enough to support the general description of the transition.

VII. HEAT-CAPACITY MEASUREMENTS

Heat-capacity measurements over the range 4—300 K were carried out using a computer-controlled adiabatic calorimeter system which has been described in detail elsewhere.[19,20] The absolute error of this system was deter-

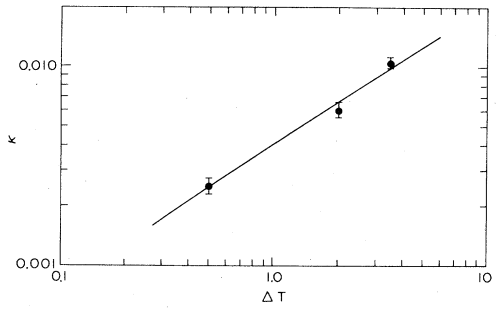

FIG. 8. Log-lot plot of the temperature dependence of the inverse range parameter κ on $T-T_N$. The line corresponds to a value of the critical index ν equal to 0.72 ± 0.08, with $T_N=289.5$ K.

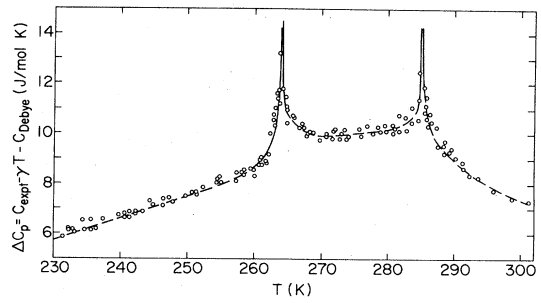

FIG. 9. Temperature dependence of the magnetic specific heat. The solid lines represent a nonlinear least-squares fit, as explained in the text.

mined to be less than 0.5% using National Bureau of Standards (NBS) standard samples of Cu and benzoic acid. The electronic heat-capacity coefficient γ was determined using a computer-controlled pulse calorimeter operating over the range 1.5—10 K with an accuracy of less than 1%.

The total heat capacity, as determined in this work, is consistent with the results reported by Mikhel'son *et al.*[11]; however, the resolution and precision of the present data are considerably improved with respect to those reported earlier. In order to extract the magnetic contribution to the heat capacity we measured the heat capacity over the range 1.5—300 K. This allowed for the evaluation of both the electronic and lattice contributions. The electronic heat-capacity coefficient γ was determined to be 0.0043 J/mol K^2. The lattice contribution was evaluated by determining the value of Θ_D as a function of temperature from the data below 80 K and extrapolating smoothly to 300 K. These values of Θ_D were then used to calculate the lattice contribution to the heat capacity up to 300 K. The magnetic contribution, given by $C_M=C_{\text{expt}}-\gamma T-C_{\text{Debye}}$, is shown in Fig. 9. These data exhibit two λ-like anomalies occurring at 264.0 and 285.0 K. The solid lines indicate the results of a gradient expansion nonlinear least-squares fit to the equation

$$C_M=A+B\left|\frac{T-T_N}{T_N}\right|^{-\alpha}.$$

Both anomalies can be fitted, to within the indicated errors, with $A=1.692\pm0.001$, $B=3.516\pm0.001$ and $\alpha=0.159\pm0.001$. The results of this treatment are consistent with both transitions being of second order. The transition temperatures are consistent with those reported by Mikhel'son *et al.*,[11] but are slightly higher than those given by the neutron measurements.

In order to ascertain that there was in fact no latent heat associated with either transition, the amount of energy required to cover a 10-K range spanning each transition, was measured to determine the enthalpy change. In each case the value of the enthalpy determined in this manner agreed, within experimental error, with that obtained from an integration of the heat-capacity data over the same temperature range. This agreement leads to the conclusion that the heat-capacity results show evidence for only second-order transitions at both temperatures.

The entropy associated with the magnetic heat capacity up to 300 K has been determined to be 4.73 J/mol K^2. This is to be compared to R ln2 as expected from the measured magnetic moment of $1.2\mu_B$ determined from the neutron studies. Thus 82% of the expected entropy is achieved by the magnetic system at 300 K.

VIII. SYMMETRY AND RENORMALIZATION-GROUP CONSIDERATIONS

In this section we construct a Landau-Ginzburg-Wilson (LGW) model associated with $FeGe_2$. The expected magnetic structure and the phase diagram of this model are then analyzed using mean-field and renormalization-group considerations. We first consider the zero magnetic field case and then analyze the phase diagram in the presence of an external magnetic field.

A. $H=0$

The neutron-diffraction studies presented in this work suggest that the low-temperature phase of $FeGe_2$ is associated with a two-component order parameter

$$A_x=S_{1x}-S_{2x}+S_{3x}-S_{4x}\,,$$
$$A_y=S_{1y}-S_{2y}+S_{3y}-S_{4y}\,. \tag{1}$$

Here $(S_{ix},S_{iy}),i=1,\ldots,4$ is the spin vector associated with the Fe ion at site i (see Fig. 1). In the intermediate phase this order parameter becomes modulated, with propagation vector $\mathbf{q}$ along [100] and [010]. Such a phase may be described by one of the following order parameters: (a) A transversely polarized spin-density-wave (SDW) order parameter

$$\Psi^T_{x,\pm q}=A_x e^{\pm iqy}\,,$$
$$\Psi^T_{y,\pm q}=A_y e^{\pm iqx}\,, \tag{2}$$

and (b) a longitudinally polarized SDW order parameter

$$\Psi^L_{x,\pm q}=A_x e^{\pm iqx}\,,$$
$$\Psi^L_{y,\pm q}=A_y e^{\pm iqy}\,. \tag{3}$$

Each of these order parameters has $n=4$ components.

Note that the two order parameters belong to two different irreducible representations of the paramagnetic symmetry group of $FeGe_2$ (D_{4h}^{18}). Therefore, if the transition from the paramagnetic to the intermediate phase is continuous, then one expects that the magnetic structure of the intermediate phase should be given by one of these order parameters (and not both). However, if the spin anisotropy is negligible,[21] the two order parameters become degenerate. We will consider this possibility at the end of this section. We assume now that the order parameter is Ψ^T. In order to analyze the magnetic structure of the intermediate phase we define the following real order parameters $\phi_i, \bar{\phi}_i$, $i=1,2$:

$$\Psi^T_{x,\pm q} \equiv \phi_1 \pm i\bar{\phi}_1 ,$$
$$\Psi^T_{y,\pm q} \equiv \phi_2 \pm i\bar{\phi}_2 . \tag{4}$$

The LGW model associated with the para-intermediate transition takes the form

$$\frac{\mathscr{H}}{k_B T} = \tfrac{1}{2} r \sum_{i=1}^{2} (\phi_i^2 + \bar{\phi}_i^2) + \tfrac{1}{2} \sum_{i=1}^{2} [(\nabla\phi_i)^2 + (\nabla\bar{\phi}_i)^2] + u \left[\sum_{i=1}^{2} \phi_i^2 + \bar{\phi}_i^2 \right]^2 + v \sum_{i=1}^{2} (\phi_i^2 + \bar{\phi}_i^2)^2 . \tag{5}$$

Minimizing this Hamiltonian with respect to ϕ_i and $\bar{\phi}_i$, one finds that for $v<0$ a transversely polarized SDW structure (namely, a structure for which $\langle \Psi^T_{x,\pm q} \rangle \neq 0$ but $\langle \Psi^T_{y,\pm q} \rangle = 0$) is favored. On the other hand for $v>0$ a multi-q structure is favored. Here both $\langle \Psi^T_{x,\pm q} \rangle$ and $\langle \psi^T_{y,\pm q} \rangle$ are nonzero in the same domain. Within the Landau theory both structures may be associated with a continuous para-intermediate transition.

However, renormalization group (RG) calculations yield further restrictions on the possible magnetic structure. RG studies of the model (5) in $d=4-\epsilon$ ($\epsilon>0$) dimensions show[22] that this model has a stable fixed point which satisfies $v^*>0$ to second order in ϵ. This suggests that if the para-intermediate (i.e., para-incommensurate) transition is second order, then the magnetic structure is described by a multi-q spin arrangement.

The model (5) is associated with the para-incommensurate transition. We now construct a more general LGW model which may describe both the para-incommensurate and incommensurate-commensurate transitions. Let A_x, A_y be the order parameters defined in Eq. (1). Consider the following Landau-Ginzburg model:

$$\frac{1}{k_B T}\mathscr{H}_0 = \frac{1}{2} r (A_x^2 + A_y^2) + \frac{1}{2}\alpha \left[\left[\frac{dA_x}{dy} \right]^2 + \left[\frac{dA_y}{dx} \right]^2 \right] + \frac{1}{2} \left[\left[\frac{d^2 A_x}{dy^2} \right]^2 + \left[\frac{d^2 A_y}{dx^2} \right]^2 \right] + \bar{u}(A_x^2 + A_y^2)^2 + \bar{v}(A_x^4 + A_y^4) . \tag{6}$$

Minimizing (6) we find that this model exhibits a para-commensurate (antiferromagnetic) transition at $r=0$ for $\alpha>0$ and a para-incommensurate transition at $r=\frac{1}{4}\alpha^2$ for $\alpha<0$. The two ordered phases are separated by a first-order line. The fact that this line is first order is due to the anisotropic term $\bar{v}$ in the Hamiltonian.[23] The three transition lines join at a Lifshitz point (see Fig. 10). Note that the discontinuity of the order parameter along the first-order commensurate-incommensurate line is expected to vanish as one approaches the Lifshitz point. Therefore, in the vicinity of this point the commensurate-incommensurate transition is expected to be weakly first order. In applying the model (6) to a concrete physical system, one should consider temperature-dependent parameters r and α. In the case of $FeGe_2$, the parameters might be such that as one lowers the temperature, one finds a para-incommensurate transition followed by a weakly first-order incommensurate-commensurate transition.

The experimental results discussed in the preceding section suggest that the magnetic structure of the intermediate phase is composed of *both* transverse and longitudinal order parameters Ψ^T and Ψ^L. Within the Landau theory, such a structure may indicate that the para-intermediate transition either (a) is first order or (b) splits into two second-order transitions each of which is associated with one order parameter (either Ψ^T or Ψ^L). Experimentally it may not be easy to observe the two transitions if they are close to each other, or to detect a discontinuity in the transition if it is only weakly first order. The fact that the intermediate phase seems to be obtained from the paramagnetic phase by a single continuous transition, indicates that the two order parameters Ψ^T and Ψ^L are almost degenerate. In order to study this possibility, we consider the phase diagram assuming that the in-plane spin anisotropy is negligible and may be ignored—in this case the two ($n=4$)-component order parameters Ψ^T and Ψ^L form a single 8-component vector. Let

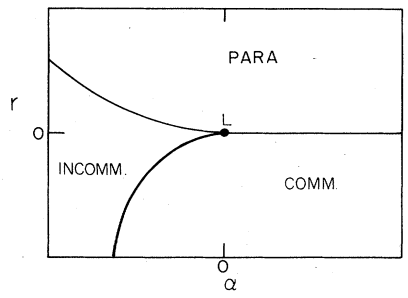

FIG. 10. (r,α) phase diagram of the model (6), obtained within the mean-field approximation. The model exhibits three phases: paramagnetic, commensurate, and incommensurate, separated by three lines. The three lines join at a Lifshitz point L. Here and in Figs. 11 and 12 thin lines represent second-order transitions and thick lines, first-order transitions. Note that in the zero spin-anisotropy case the commensurate-incommensurate line is second order and not first order as shown (see text).

$$\Psi_{\pm 1}=\mathbf{A}e^{\pm iqx},$$
$$\Psi_{\pm 2}=\mathbf{A}e^{\pm iqy},$$

be the 8 components of the order parameter. Here $\Psi_{\pm 1}$ and $\Psi_{\pm 2}$ describe SDW with propagation vector along the x and y axes, respectively. The LGW model associated with this order parameter has four fourth-order invariants, and it takes the form

$$\frac{1}{k_B T}\mathscr{H}=\tfrac{1}{2}r(\Psi_1\cdot\Psi_{-1}+\Psi_2\cdot\Psi_{-2})+\tfrac{1}{2}(\nabla\Psi_1\cdot\nabla\Psi_{-1}+\nabla\Psi_2\cdot\nabla\Psi_{-2})+u_1[(\Psi_1\cdot\Psi_{-1})^2+(\Psi_2\cdot\Psi_{-2})^2]$$
$$+u_2(\Psi_1\cdot\Psi_{-1})(\Psi_2\cdot\Psi_{-2})+\tfrac{1}{4}z[(\Psi_1\cdot\Psi_1)(\Psi_{-1}\cdot\Psi_{-1})-(\Psi_1\cdot\Psi_{-1})^2+(\Psi_2\cdot\Psi_2)(\Psi_{-2}\cdot\Psi_{-2})-(\Psi_2\cdot\Psi_{-2})^2]$$
$$+\tfrac{1}{2}w[(\Psi_1\cdot\Psi_2)(\Psi_{-1}\cdot\Psi_{-2})+(\Psi_1\cdot\Psi_{-2})(\Psi_{-1}\cdot\Psi_2)].$$

The phase transition associated with this model may be studied by renormalization-group calculations. We find the following recursion relations to first order in $\epsilon=4-d$, where d is the dimensionality of the system:

$$\frac{du_1}{dl}=\epsilon u_1-k_4(48u_1^2+4u_2^2+z^2-4u_1z+2w^2+4wu_2),$$
$$\frac{du_2}{dl}=\epsilon u_2-k_4(8u_2^2+48u_2u_1-4u_2z+2w^2+16wu_1-4wz),$$
$$\frac{dz}{dl}=\epsilon z-k_4(-8z^2+48u_1z+4w^2),$$
$$\frac{dw}{dl}=\epsilon w-k_4(8w^2+16wu_1+16wu_2+4wz).$$

Here k_4 is a constant. These recursion relations do not have a real, stable fixed point. In particular we find that all fixed points with $w^*=0$ are unstable to perturbations of w, while all the fixed points with $w^*\neq 0$ are complex, and therefore not physically accessible. This analysis suggests that the para-intermediate transition is expected to be first order.

By minimizing the LGW Hamiltonian, one obtains the order parameter in the intermediate phase. The resulting magnetic structure (whether it is, for example, single-**q**, multi-**q**, linearly polarized SDW or a spiral) depends on the parameters u_1, u_2, z, and w which define the model. These parameters are not easy to calculate, and one needs a detailed microscopic model for the magnetic interactions in $FeGe_2$ in order to estimate them. However, one can get a rough estimate of these parameters, if one assumes that the LGW Hamiltonian is derived from the model (6), with $\bar{v}=0$. Here, all four terms u_1, u_2, z, and w are obtained from the single fourth-order term, $\bar{u}(A_x^2+A_y^2)^2$, which appears in (6). In order to calculate u_1, u_2, z, and w one has to Fourier transform the $\bar{u}$ term in (6). We find $u_1=6\bar{u}$, $u_2=8\bar{u}$, $z=8\bar{u}$, and $w=16\bar{u}$. It can be verified that the magnetic structure which minimizes this Hamiltonian is a single-**q** planar spiral, namely, a structure for which $\Psi=\hat{\mathbf{x}}+i\hat{\mathbf{y}}$ and $\Psi_2=0$; where $\hat{\mathbf{x}}$ and $\hat{\mathbf{y}}$ are unit vectors along the x and y axes, respectively.

In summary, we find that the para-intermediate phase transition is not expected to be continuous even if the basal-plane spin anisotropy is neglected. The experimental observation, that the intermediate phase is composed of both transverse and longitudinal order parameters indicates that these order parameters are almost degenerate. Simple considerations indicate that the magnetic structure may be a single-**q** planar spiral, in agreement with the observed magnetic reflections.

B. $H\neq 0$

In this section we consider the (H,T) phase diagram of a model corresponding to $FeGe_2$, with $\mathbf{H}\|[100]$. The LGW model takes the form

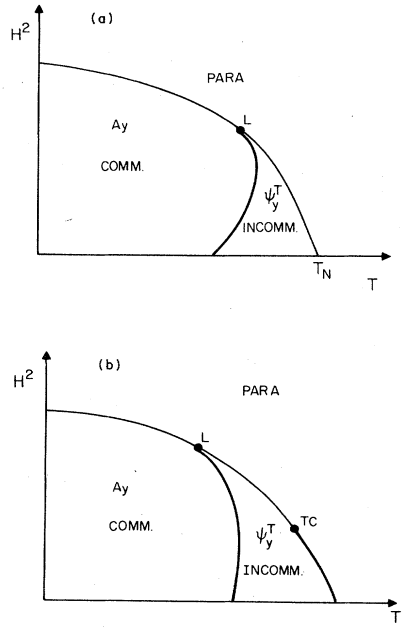

FIG. 11. Schematic (H^2,T) phase diagram associated with the model (7) for $v\leq 0$, (a) obtained by mean-field calculations and (b) consistent with the renormalization-group arguments. In this case the incommensurate phase exhibits a single-q structure. TC is a tricritical point and L is a Lifshitz point.

$$\mathcal{H}=\mathcal{H}_0+\mathcal{H}_1 \tag{7}$$

where $\mathcal{H}_0$ is the LGW Hamiltonian in zero external field given by Eq. (6) and

$$\frac{1}{k_B T}\mathcal{H}_1=aH^2(A_x^2-A_y^2) \tag{8}$$

describes the coupling of the antiferromagnetic order parameter to the external magnetic field. Here a is a constant. The magnetic field H favors ordering of A_y (rather than A_x) in the low-temperature, commensurate phase and ordering of $\Psi^T_{y,\pm q}$ (rather than $\Psi^T_{x,\pm q}$) in the incommensurate phase. The other term which affects the magnetic structure in the ordered phase is the cubic anisotropy v. The (H,T) phase diagram will be affected rather drastically by the sign of v. Consider first the case $\bar{v}<0$. Here the cubic anisotropy favors ordering along [10] or [01] (but not along [11] or [$\bar{1}$1]) in the antiferromagnetic phase. It also favors a single-q structure in the intermediate phase. Therefore, in this case, the magnetic field and the cubic anisotropy are not competing but rather they favor the same type of ordering in both phases. The expected mean-field phase diagram is given schematically in Fig. 11(a). This phase diagram displays second-order para-commensurate and para-incommensurate lines and a first-order commensurate-incommensurate transition. The three lines join at a Lifshitz point L. This phase diagram is expected to be valid also for the case in which the the cubic anisotropy favors ordering along [10] or [01] (but not along [11] or [$\bar{1}$1]) in the antiferromagnetic phase. It also favors a single-q structure in the intermediate phase. Therefore, in this case, the magnetic field and the cubic anisotropy are not competing but rather they favor the same type of ordering in both phases. The expected mean-field phase diagram is given schematically in Fig. 11(a). This phase diagram displays second-order para-commensurate and para-incommensurate lines and a first-order commensurate-incommensurate transition. The three lines join at a Lifshitz point L. This phase diagram is expected to be valid also for the case in which the cubic anisotropy v is taken to be zero. Within the RG approach the para-incommensurate transition at $H=0$ is first order since the incommensurate phase exhibits a single-**q** structure. We thus expect that the para-incommensurate transition is first order not only at $H=0$ but also for sufficiently small H. At larger H the transition may become continuous via, for example, a tricritical point. A simple phase diagram consistent with these considerations is given in Fig. 11(b).

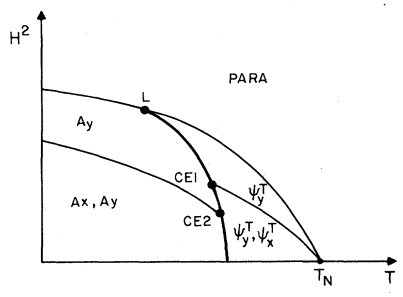

FIG. 12. Same as Fig. 11 but for $v>0$. Here the model exhibits five phases: paramagnetic, two incommensurate phases with single-q and multi-q structures, respectively, and two commensurate phases with magnetic structures given by A_y and (A_y,A_x) respectively. CE1 and CE2 are two critical end points. Here T_N is a tetracritical point.

Consider now the case $v>0$. Here the cubic anisotropy favors ordering along [11] or [$\bar{1}$1] in the commensurate phase, and multi-q structure in the incommensurate phase. The cubic anisotropy, therefore, competes with the magnetic field. In this case one expects that at finite field, the para-incommensurate transition should split into two transitions: first a transition associated with $\Psi^T_{y,\pm q}$ and then, at a lower temperature, a transition in which $\Psi^T_{x,\pm q}$ orders as well. Similarly the para-commensurate transition should also split into two transitions associated with A_y and A_x, respectively. A schematic (T,H) phase diagram consistent with these considerations is given in Fig. 12.

ACKNOWLEDGMENTS

We acknowledge the assistance of Mr. Kuyler Wise in the determination of the heat capacity. This research was carried out at Brookhaven National Laboratory under Contract No. DE-AC02-76CH00016 with the U.S. Department of Energy and supported by its Division of Materials Sciences, Office of Basic Energy Sciences, and supported in part by a grant from the Israel Academy of Sciences and Humanities—Basic Research Foundation.

*Present address: Fujian Institute of Research on the Structure of Matter, Chinese Academy of Sciences, Fuzhou, Fujian, China.

[1]H. J. Wallbaum, Z. Metallknd. **35**, 218 (1943).
[2]K. Yasukochi, K. Kanematsu, and T. Ohoyama, J. Phys. Soc. Jpn. **16**, 429 (1961).
[3]G. Airoldi and R. Pauthenet, C. R. Acad. Sci. Paris **258**, 3994 (1964).
[4]E. Krén and P. Szabó, Phys. Lett. **11**, 215 (1964).
[5]J. B. Forsyth, C. E. Johnson, and P. J. Brown, Philos. Mag. **10**, 713 (1964).
[6]N. S. Satya Murthy, R. J. Begum, C. S. Somanathan, and M. R. L. N. Murthy, Solid State Commun. **3**, 113 (1965).
[7]E. F. Bertaut and J. Chenavas, Solid State Commun. **3**, 117 (1965).
[8]E. Adelson and A. E. Austin, Bull. Am. Phys. Soc. **10**, 352 (1965); see also J. Phys. Chem. Solids **26**, 1975 (1965).
[9]J. Sólyom and E. Krén, Solid State Commun. **4**, 255 (1966).

[10]R. P. Krentsis, A. V. Mikhel'son, and P. V. Gel'd, Fiz. Tverd. Tela (Leningrad) **12**, 933 (1970) [Sov. Phys.—Solid State **12**, 727 (1970)].

[11]A. V. Mikhel'son, R. P. Krentsis, and P. V. Gel'd, Fiz. Tverd. Tela (Leningrad) **12**, 2470 (1970) [Sov. Phys.—Solid State **12**, 1979 (1971)].

[12]I. N. Sachkov, R. P. Krentsis, and P. V. Gel'd, Fiz. Tverd. Tela (Leningrad) **12**, 2819 (1977) [Sov. Phys.—Solid State **19**, (1977)].

[13]I. I. Piratinskaya, A. V. Mikhel'son, and R. P. Krentsis, Fiz. Tverd. Tela (Leningrad) **21**, 1833 (1979) [Sov. Phys.—Solid State **21**, 1050 (1979)].

[14]G. P. Zinov'eva, A. V. Mikhel'son, L. P. Andreeva, R. P. Krentsis, and P. V. Gel'd, Fiz. Tverd. Tela (Leningrad) **14**, 1578 (1972) [Sov. Phys.—Solid State **14**, 1364 (1972)].

[15]K. P. Belov, *Magnetic Transitions* (Consultants Bureau, New York, 1961) (translated from the Russian).

[16]H. Bennett, Phys. Rev. **185**, 801 (1969).

[17]V. Pluzhnikov, D. Feder, and E. Fawcett, J. Magn. Magn. Mater. **27**, 343 (1982).

[18]Note that L_1 and L_3 appear to have been inadvertently interchanged in Eqs. (a) and (b) of their paper, and a factor of 2 has been omitted in calculating moments.

[19]D. J. Germano, R. A. Butera, S. G. Sankar, and K. A. Gschneidner, Jr., J. Appl. Phys. **50**, 7495 (1979).

[20]D. J. Germano, Ph.D. thesis, University of Pittsburgh, 1980.

[21]See for example, S. A. Brazovskii and J. E. Dzyaloshinsky, Pis'ma Zh. Eksp. Teor. Fiz. **21**, 360 (1975) [JETP—Lett. **21**, 164 (1975)].

[22]D. Mukamel, Phys. Rev. Lett. **34**, 481 (1975).

[23]A. Michelson, Phys. Rev. B **16**, 577 (1977); **16**, 585 (1977); **16**, 5121 (1977).